State-Based Control of Primary–Standby Battery Switching in Standalone Photovoltaic Systems

Manuscript received July 1, 2026; revised August 5, 2026

Reza Satria Rinaldi*
Dept. of Electrical Engineering
University of Bengkulu
Bengkulu, Indonesia
reza_s_r@unib.ac.id

Afriyastuti Herawati
Dept. of Electrical Engineering
University of Bengkulu
Bengkulu, Indonesia
afriyastuti_herawati@unib.ac.id

Ika Novia Anggraini
Dept. of Electrical Engineering
University of Bengkulu
Bengkulu, Indonesia
ikanovia@unib.ac.id

Melian Tri Yulianto
Dept. of Electrical Engineering
University of Bengkulu
Bengkulu, Indonesia
mtyulianto2003@gmail.com

Abstract*—Off-grid photovoltaic (PV) systems are a viable solution for electrifying remote areas. However, the intermittent nature of solar energy necessitates the use of properly managed batteries to ensure a continuous power supply and preserve battery lifespan. While various battery control systems have been developed, most rely on relatively complex digital controls, making them less suitable for small-scale household applications. This study aims to develop an automatic switching system for charging and discharging between primary and standby batteries in a 12 V DC standalone PV (SAPV) system, utilizing state-based control logic. The proposed system employs two Valve-Regulated Lead-Acid (VRLA) batteries, two Low-Voltage Disconnects (LVDs), and three electromechanical relays (EMRs) to control charging and discharging operations based on battery voltage, which represents the State of Charge (SoC) and Depth of Discharge (DoD). The control system features four operating states and eight state transitions, prioritizing full charge-discharge cycles for the primary battery while utilizing the standby battery to maintain power supply continuity during the primary battery's charge. Test results demonstrate that the system successfully automates operational switching in accordance with the designed control strategy, thereby preserving the primary battery's full cycling and ensuring continuous power supply. The system is simple, cost-effective, and easy to implement using LVDs and EMRs. Observed transition voltages do not always align exactly with the set threshold values because of the dynamic characteristics of VRLA batteries.

Keywords—automatic switching, electromechanical relays (EMRs), Low-Voltage Disconnect (LVD), standalone PV(SAPV).

I. INTRODUCTION

Geographical constraints and a dispersed population pose significant challenges in meeting the electricity needs of communities in remote areas far from the main grid (on-grid). This situation makes building an interconnection infrastructure to the main grid very expensive. Utilizing solar energy through stand-alone photovoltaic systems is one solution to overcome these constraints. This solution is considered highly feasible—technical, economic, and environmental—especially to support the domestic and economic needs of residents [1]-[6]. Furthermore, the increasingly competitive cost trend of PV technology makes this option even more promising if managed optimally [7].

The use of solar PV continues to grow due to its advantages over other renewable energy sources. However, the intermittency of solar energy sources due to weather and environmental conditions is a major problem. This results in fluctuations in the solar irradiance received by PV modules and environmental conditions, which can lead to low efficiency [8]. Therefore, the sustainability of electrical energy supply must be guaranteed in domestic applications of off-grid PV systems. Batteries for electrical energy storage are an important component in achieving this, especially when solar irradiation is low or even nonexistent [9], [10], [11].

VRLA batteries are widely used in domestic applications of off-grid PV systems. The low initial investment is a major consideration in using VRLA [12], [13]. However, there are limitations to the use of these batteries, particularly regarding their lifespan. Improper management can degrade VRLA battery lifespan, thereby increasing system maintenance costs and decreasing system reliability. Simultaneous charging and discharging, overcharging, overdischarging, repeated shallow cycles, incomplete charging, and prolonged undercharging of these batteries should be avoided to prevent degradation and increase their lifespan batteries [14]-[17].

To prevent degradation and increase battery lifespan, several studies have examined the application of battery usage control systems in off-grid PV systems. These studies examined battery charging control, power management, and power protection (voltage and current limits). Based on the research results, the reliability of the battery supply and the quality of electrical energy from batteries can be improved by implementing these control systems. Most of these studies use digital control based on microcontrollers, embedded systems, or other digital devices that use complex algorithms [11], [18]-[24]. However, their implementation requires hardware and software development, which can increase the system's complexity and investment requirements. This condition is a challenge in itself, especially in small-scale household applications requiring simple, economical solutions.

Electromechanical relay-based control systems have advantages that are often overlooked. These advantages include: circuit simplicity, ease of maintenance, and very

 EISSN: 2961-872X ●PISSN: 2961-8924●DOI: 10.56741/IISTR.esl.002471

affordable implementation costs. In addition, this control system does not require a programmable control unit, thus reducing system complexity. The electromechanical relay used in this control system is widely available. With inherent electrical isolation, the relay provides high reliability in low-voltage DC applications and is suitable for off-grid environments [25]. Although the performance of electromechanical relays is affected by contact conditions, spring characteristics, and magnetic system properties, these relays still provide reliable operation and satisfactory accuracy when properly configured, maintained, and applied according to the specified operating conditions [26].

Based on the description, this study designs a low-cost autonomous primary-standby battery switching system for a small-scale stand-alone PV (SAPV) system using an electromechanical relay (EMR) as the actuator. The uniqueness of this research lies in the implementation of a primary-standby battery control strategy that prioritizes a full charge-discharge cycle on the primary battery. The standby battery will discharge when the primary battery is charged. This control system is designed to charge and discharge two batteries that operate alternately automatically. The use of these two batteries aims to reduce stress on them and maintain continuity of the SAPV system's energy supply. The Low-Voltage Disconnect (LVD) generates a control signal for the EMR based on the voltage of the primary and standby batteries.

II. METHODS

This research is an applied study oriented towards solving practical problems in implementing automatic switching technology for primary-standby batteries in a 12 V DC small-scale SAPV system. The method used is systems analysis and design, with a focus on developing a design based on state control logic. The energy source selection mechanism for charging and discharging primary-standby VRLA batteries is adaptively determined by battery voltage, prioritizing a full charge-discharge cycle on the primary battery. The research stages include system requirements analysis, flow diagram preparation, block diagram design, state table preparation to represent the applied control logic, and wiring diagram design.

The novelty of this research lies in the design of a finite-state control logic that clearly separates the charging and discharging modes of two VRLA batteries operating as primary and standby batteries. The control system is developed using a combination of LVD and EMR devices that are simple, economical, and easy to implement. The main contribution of this research is a control system design that enables coordinated management of VRLA battery operations, that is, a switching mechanism between charging and discharging modes on primary-standby batteries, so that the continuity of power supply to the load in a small-scale SAPV system can be maintained optimally.

The proposed small-scale SAPV system uses two VRLA batteries: a primary battery and a standby battery. The battery control system automatically switches batteries between the charging and discharging modes. The work process algorithm of the battery control system is presented in the flowchart in Fig. 1. Fig. 2 illustrates the system block diagram, which consists of a PV charging system, a two-battery configuration, and a battery control system. The system input is an electrical energy source that uses solar energy to produce DC output power through the battery energy storage system. The proposed battery control system is designed to be simple and economical, with two main components: an LVD as a control signal generator and an EMR as an actuator. Fig. 3 presents a block diagram showing the integration of several LVDs and EMRs within the battery control system. A 12 V DC EMR was selected based on the operating voltage of the small-scale SAPV system.

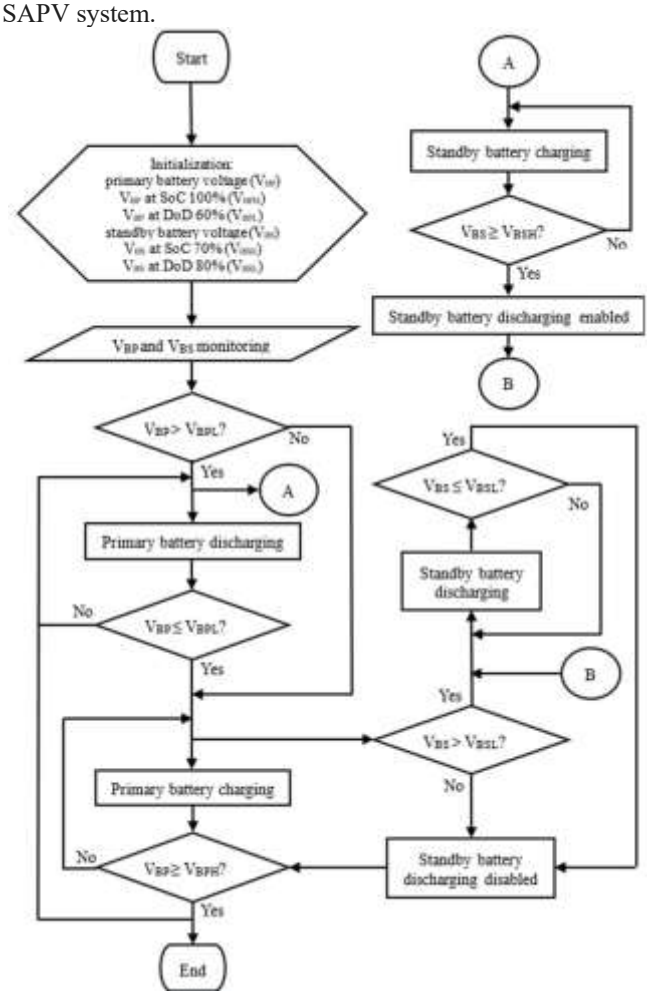


Fig. 1. Flow chart of the proposed battery control system

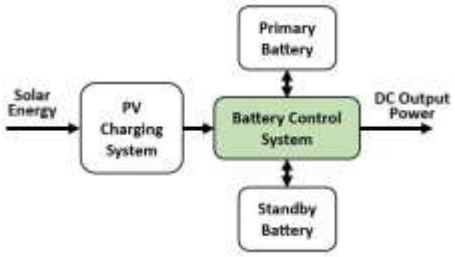


Fig. 2. Block diagram of the proposed SAPV system

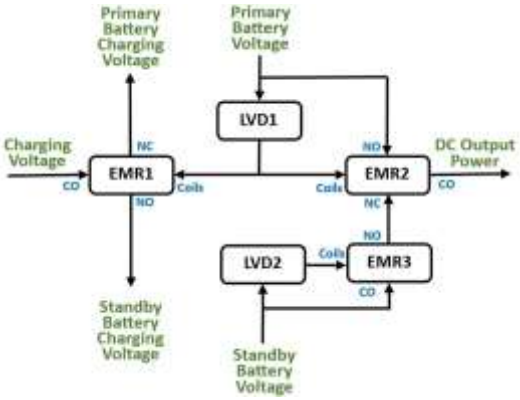


Fig. 3. Block diagram of the proposed battery control system

 EISSN: 2961-872X ●PISSN: 2961-8924●DOI: 10.56741/IISTR.esl.002471

Sulfation is a major challenge in VRLA batteries. Sulfation is one of the main causes of VRLA battery degradation. This sulfation increases the internal resistance of VRLA batteries, resulting in decreased capacity across all duty cycles. VRLA batteries are at high risk of sulfation if left at a low State of Charge (SoC) and not immediately recharged after reaching the Depth of Discharge (DoD) limit [16], [17]. In addition to sulfation, simultaneous charging and discharging of VRLA batteries can accelerate the degradation. Therefore, simultaneous charging and discharging in VRLA battery operation should be avoided [27], [28], [29]. This battery control system is designed to avoid these causes of degradation in both batteries.

The SoC and DoD parameters are usually expressed as percentages. SoC indicates the battery capacity that is still available for use, while DoD indicates the battery capacity that has been used. For example, an SoC of 100% indicates the battery is fully charged, while the DoD value at that time is 0%. Based on recommendations from VRLA battery manufacturers, the maximum DoD is 80% to ensure reliable operation and prolong battery lifespan. Nevertheless, experimental studies indicate that operating VRLA batteries at a DoD up to 60% can enhance service life [30]. In various applications requiring a direct current (DC) source from a battery, the SoC is a crucial parameter for optimizing battery usage. Since SoC cannot be measured directly, estimating its value presents a significant challenge. A correlation between SoC and the battery's internal resistance has been obtained using an SoC measurement method based on internal-resistance analysis. This internal resistance correlates with the terminal voltage and the open-circuit voltage (OCV), both of which are influenced by the current during charging and discharging [31]. To analyze the relationship between SoC and DoD as represented by the battery voltage under no-load conditions or the OCV, (1) and (2) can be used. In these equations, $V_B(t)$, V_{Bmin}, and V_{Bmax} are, respectively, the battery voltage at time t, the minimum battery voltage at 0% SoC, and the highest battery voltage at 100% SoC [25].

$$DoD\ (t) = 100\% - SoC\ (t) \tag{1}$$

$$SoC\ (t) = \frac{V_B(t) - V_{Bmin}}{V_{Bmax} - V_{Bmin}} \cdot 100\% \tag{2}$$

The SoC or DoD parameters of each battery are represented using the battery voltage read by the LVD input. The battery voltage is the LVD input voltage, which will be forwarded as the LVD output voltage. This LVD output voltage will be applied to the EMR Coils terminal as a control signal. On each LVD, the lowest (V_{BL}) and highest (V_{BH}) battery voltage limits are set to produce a control signal. The LVD will disconnect the output voltage or not produce an output voltage when the input voltage is less than V_{BL}. Thus, no voltage is applied to the EMR Coils terminal as a control signal. The LVD restores the output voltage when the battery voltage is greater than or equal to V_{BH}. Therefore, the EMR Coils terminal receives the same voltage as the battery voltage. This LVD output voltage will remain until the battery voltage reaches V_{BL}, and then the LVD output voltage will be disconnected again when the LVD input voltage is smaller than V_{BL}.

Applying a load to a VRLA battery results in a measured terminal voltage (V_T)—recorded while the battery is supplying the load—that is lower than the OCV. The difference between these two voltages falls within the range of 0.22–0.74 V. At V_T values of ≥ 11.64 V, the relationship between V_T and OCV exhibits a linear trend with a relatively constant gradient approaching 1 and a negligible offset. Conversely, when V_T < 11.64 V, the relationship between the two variables becomes more volatile, allowing it to be estimated using (3) [32]. Based on (3), V_{BL} can be determined using the V_T value calculated via (4), which approximates the OCV value at the moment of load disconnection.

$$OCV = 0.5\ V_T + 6.02 \tag{3}$$

$$V_T = 2\ (OCV - 6.02) \tag{4}$$

TABLE I. LVD OPERATING STATES AND CORRESPONDING EMR CONTROL SIGNALS

Battery voltage (V_B)	LVD Voltage		Control Signal
	Input (V_{in})	*Output (V_{out})*	
Decreases from ≥ V_{BH} to V_{BL}	V_B	V_{in}	1
< V_{BL} and Increases from < V_{BL} to > V_{BH}	V_B	0	0

The LVD input and output voltages and control signals for the EMR Coils terminal are shown in Table I. The EMR control signal generated from the LVD output voltage is represented as binary logic 0 when there is no voltage and 1 when there is a voltage from the LVD output. In the battery control system design, as shown in Fig. 3, 2 LVDs are used: LVD1 and LVD2. The input terminal of LVD1 detects a primary battery voltage, while the input terminals of LVD2 detect a standby battery voltage. LVD1 will generate a control signal for EMR1 and EMR2; LVD2 will generate a control signal for EMR3. LVD1 generates a control signal to maintain a full charge-discharge cycle on the primary battery and prevent simultaneous charge-discharge operations on both the primary and the standby batteries. With the control signal from LVD1, EMR2 will activate the primary battery discharge mode by connecting the battery to the load from DoD 0% to 60%. Conversely, EMR1 will activate the charge mode on the standby battery by connecting it to the battery terminal of the Solar Charge Controller (SCC) in the PV charging system. When the primary battery is in charging mode, the load supply will be switched by EMR2 to the standby battery. Conversely, when the primary battery is in discharging mode, the battery terminal SCC will be switched by EMR1 to connect to the standby battery. The SCC must always be connected to the battery to prevent initialization errors, system voltage detection errors, or even damage to the SCC's internal electronic circuits. To optimize the power supply to the load when the primary battery is in charging mode while maintaining the standby battery's lifetime, EMR3, based on the control signal provided by LVD2, will cut off the standby battery's power supply to the load when the DoD is 60%, or the SoC is 40%. When the standby battery's SoC reaches 80%, it will resume supplying power to the load.

EMR is a basic electromagnetic device in a control system. The EMR structure, as shown in Fig. 4, generally consists of an iron core, coil, armature, return spring, and contact system. The contact system in this EMR consists of NO (normally open), NC (normally closed), and CO (common) contacts. The Electromagnetic force (magnetic field) will occur when a certain voltage is applied to the coil through the EMR coil terminals. As a result, the armature is attracted to the iron core because the electromagnetic force is greater than the spring force of the return spring, so the CO contact is connected to the NO contact, or the CO contact is

disconnected from the NC contact. The operation of the EMR when voltage is applied to the coil terminals is illustrated in Fig. 5. The opposite condition occurs when the voltage is not applied or disconnected from the EMR coil terminals. The armature will return to its original position, as shown in Fig. 4, so the CO contact is connected to the NC contact, or the CO contact is disconnected from the NO contact [33]. The fundamental operating principle of AC and DC EMRs is identical, although they differ in coil design and magnetic circuit construction. In general, the recommended operating voltage range for EMR is 80% to 110% of the EMR coil's nominal voltage.

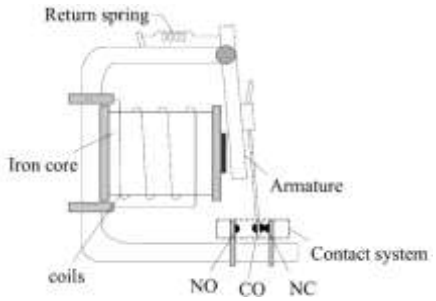


Fig. 4. The structure of EMR [33]

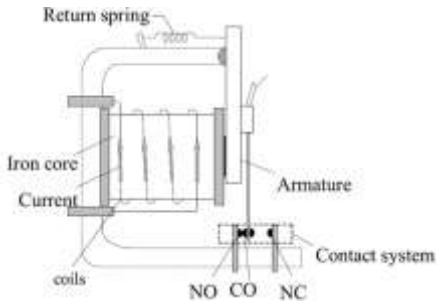


Fig. 5. EMR is energized [33]

In this design, EMR1 and EMR2 are SPDT (Single Pole Double Throw) types, each with a coil terminal and 3 contact terminals: CO, NO, and NC. EMR3 is an SPST (Single Pole Single Throw) type consisting of a coil terminal and 2 contact terminals: CO and NO. In the SPDT type EMR, when a control signal of 1 is applied to the EMR Coils terminal, the CO contact will be connected to the NO contact, and the CO contact will be connected to the NC contact when a control signal of 0 is applied to the EMR Coils terminal. While in the SPST type EMR, when a control signal of 1 is applied at the EMR Coils terminal, the CO contact will be connected to the NO contact, and the CO contact is not connected to the NO contact when a control signal of 0 is applied to the EMR Coils terminal. EMR1 and EMR2 are used for battery selection during charging and discharging operations, respectively, whereas EMR3 enables standby battery discharging based on predefined SoC thresholds. The operating modes of EMR1, EMR2, and EMR3 are presented in Tables II-IV.

TABLE II. EMR1 CHARGING SELECTION MODES

Control Signal	Contact State	System Operation
1	CO connected to NO	Standby battery charging
0	CO connected to NC	Primary battery charging

TABLE III. EMR2 DISCHARGING SELECTION MODES

Control Signal	Contact State	System Operation
1	CO connected to NO	Primary battery discharging
0	CO connected to NC	Standby battery discharging

TABLE IV. EMR3 MODES FOR STANDBY BATTERY DISCHARGE CONTROL

Control Signal	Contact State	System Operation
1	CO connected to NO	Discharge enabled
0	CO disconnected from NO	Discharge disabled

Tables II-IV describe the operation modes of EMR1, EMR2, and EMR3 separately. In the proposed battery control strategy, the operation of EMR1, EMR2, and EMR3 is not independent. Rather, the switching state of each EMR is determined by the collective state of all EMRs in response to the applied control signals. Consequently, the coordinated operation of EMR1, EMR2, and EMR3 leads to several distinct operating states within the proposed battery control system. The control signals applied to EMR1 and EMR2 are the same because they are sourced from LVD1 with the same V_{BH} and V_{BL} settings. Possible operating states of the proposed battery control system are presented in Table V.

TABLE V. POSSIBLE SYSTEM OPERATING STATES

Control Signal from LVD1 and LVD2		State	Battery operation	
			Primary	*Standby*
1	1	S1	Discharging	Charging
1	0	S2	Discharging	Charging
0	1	S3	Charging	Discharging
0	0	S4	Charging	Waiting to charge

Table V shows that there are 4 (four) possible operating states in the proposed battery control system, namely S1-S4. Each state represents a unique combination of battery operating conditions and EMR. These possible operating states form the basis for the state transition diagram shown in Fig. 6. This diagram illustrates the dynamic behavior of the proposed battery control system. With these state transitions illustrated, the analysis of the proposed battery control strategy becomes easier. The conditions that trigger each of these state transitions are presented in Table VI.

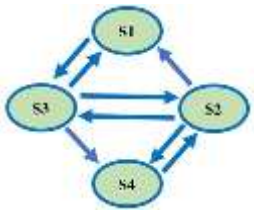


Fig. 6. The state transition diagram of the battery control system

TABLE VI. STATE TRANSITIONS

State transition	Transition condition	
	Primary battery	*Standby battery*
S1 to S3	DoD exceeds 60%	SoC remained ≥ 80%
S2 to S1	DoD remains < 60%	SoC reached 80%
S2 to S3	DoD exceeds 60%	SoC reached 80%
S2 to S4	DoD exceeds 60%	SoC remained < 80%
S3 to S1	SoC reached 100%	DoD remains < 60%
S3 to S2	SoC reached 100%	DoD exceeds 60%
S3 to S4	SoC remained < 100%	DoD exceeds 60%
S4 to S2	SoC reached 100%	SoC remained < 80%

Fig. 6 and Table VII show that there are 8 (eight) state transitions in the proposed battery control system. These state transitions occur automatically based on the DoD or SoC of the primary and standby batteries. In the primary battery transition condition, maintaining the primary battery's full charging-discharging cycle is prioritized. The primary battery will start charging once the DoD exceeds 60%, so that the

 EISSN: 2961-872X ●PISSN: 2961-8924●DOI: 10.56741/IISTR.esl.002471

battery charging cycle is maintained from 40% to 100% SoC. Likewise, the primary battery discharge cycle is maintained from 0% to 60% DoD, which begins after the SoC reaches 100%. Meanwhile, the state transition in the standby battery maintains continuity of power supply to the load while the primary battery is charging. However, the battery control system still maintains standby battery discharge until the DoD exceeds 60%, then discharges back after the SoC reaches 80%.

III. Results and Discussion

The proposed battery control system design clearly separates the charging and discharging operations of 2 (two) VRLA batteries, both the primary and the standby battery, and defines the state transition conditions that depend on the battery voltage as a representation of the SoC or DoD parameters. In addition, the charging and discharging operations of both the primary and standby batteries are performed alternately. The wiring diagram of the proposed EMR-based battery switching control system is shown in Fig. 7. The control strategy is implemented using LVDs and EMRs, resulting in a simple and cost-effective hardware architecture for automatic battery charging and discharging without a programmable controller.

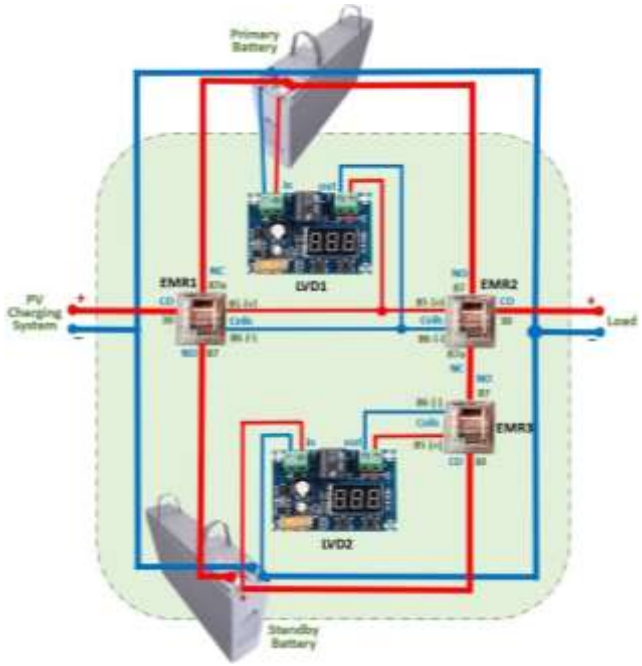


Fig. 7. Wiring diagram of the proposed battery control system

As shown in Fig. 7, the battery control system circuit comprises LVD1, LVD2, EMR1, EMR2, and EMR3, which collectively perform the battery control functions. The input terminal (in) of LVD1 is connected to the primary battery terminal to detect the primary battery voltage condition, and the input terminal of LVD2 is connected to the standby battery terminal to detect the standby battery voltage condition. The output terminal (out) of LVD1 is connected to the coil terminals (85 and 86) on EMR1 and EMR2, while the output terminal of LVD2 is connected to the coil terminals of EMR3. Through these coil terminals, each EMR will receive control signals from the output terminals of LVD1 and LVD2. When a voltage is present at the LVD output terminal, the EMR coil is energized, generating an electromagnetic force. Consequently, a logic-high (1) control signal is applied to the EMR. Conversely, when no voltage is present at the LVD output terminal, the EMR coil is de-energized, and the electromagnetic force is absent. Consequently, a logic-low (0) control signal is applied to the EMR.

At EMR1, the CO terminal (30) is connected to the SCC battery terminal as a PV energy source for battery charging; the NO terminal (87) is connected to the standby battery for charging the standby battery; and the NC terminal (87a) is connected to the primary battery for charging the primary battery. With the connection at the EMR1 terminal, the PV energy source will only charge one of the batteries, namely the primary battery, when the control signal at EMR1 is logic 0, and vice versa, the standby battery when the control signal at EMR1 is logic 1. At EMR2, the CO terminal is connected to the load as an energy source for the load; the NO terminal is connected to the primary battery as a load power supply; and the NC terminal is connected to the standby battery via the NO terminal at EMR3 as a standby load power supply. With the connection on the EMR2 terminal, the load will only be supplied alternately by one of the batteries, namely the primary battery when the control signal on EMR2 is logic 1, and vice versa, the standby battery when the control signal on EMR2 is logic 0. On EMR 3, the CO terminal is connected to the standby battery as a standby power supply; the NO terminal is connected to the load via EMR2's NC terminal when the primary battery is charging. Based on the EMR3 terminal configuration, the standby battery supplies power to the load via the NC terminal at EMR2 only when the control signal applied to EMR3 is logic 1. Conversely, the standby battery is disconnected from the load via the NC terminal at EMR2 when the control signal applied to EMR3 is logic 0.

In the proposed battery control system, two VRLA batteries are utilized to store electrical energy harvested from solar power and provide power to the load. The two batteries used in this design are 12 V, 100 Ah Shoto VRLA batteries from the 6-FMX-100B series. The battery control system, as an automatic switching technology, uses 2 (two) LVD XH-M609 units, 2 (two) SPDT 12 V 80 A EMR units, and 1 (one) SPST 12 V 80 A EMR unit. The battery voltage value representing DoD or SoC as the main control parameter is determined first using (1) and (2).

The minimum battery voltage (V_{Bmin}) at 0% SoC and the corresponding maximum battery voltage (V_{Bmax}) at 100% SoC need to be determined first. Based on the specifications given in the 12 V 100 Ah Shoto VRLA battery datasheet of the 6-FMX-100B series, V_{Bmin} can be determined first. The battery data sheet provides data on capacity 100 Ah @ 10 hours at 1.8 V per cell [34]. The minimum voltage of a six-cell VRLA battery is as follows.

$$V_{Bmin} = 6 \cdot 1.8 \text{ V} = 10.8 \text{ V}$$

V_{Bmax} is estimated by directly measuring the battery's no-load voltage, known as the open-circuit voltage (OCV) estimation method. The measurement data were obtained by charging a 12 V, 100 Ah VRLA battery with a charger from its initial voltage to full charge. The results provided by the two batteries, namely Battery A and Battery B, are presented in Table VII. V_{Bmax} is defined as the average fully charged voltage from the experimental results in Table VII: 13.20 V for Battery A and 12.74 V for Battery B. Based on these results, Battery A is the primary battery and Battery B is the standby battery in this design.

TABLE VII. RESULT OF THE EXPERIMENT OF FULLY CHARGING THE BATTERIES

Experiment to-	Battery-A Voltage (V)		Battery-B Voltage (V)	
	Initial	*Full*	*Initial*	*Full*
1	12.47	13.35	11.80	13.11
2	11.85	13.20	12.55	13.16
3	12.89	13.36	12.47	13.20
4	12.79	13.11	12.32	13.12
5	12.29	13.16	12.35	13.11
6	12.56	13.14	11.90	13.08
7	12.35	13.11	12.35	13.15
8	11.63	13.24	12.40	13.00
9	12.56	13.21	12.50	13.16
10	12.53	13.20	12.53	13.14
Average		**13.20**		**13.12**

Using (1) and (2), the voltage values of the primary battery and the standby battery, representing the SoC and DoD of each battery, can be estimated. The primary battery is allowed to discharge from DoD 0% to 60%. Accordingly, the primary battery voltage corresponding to DoD 60% (SoC 40%) is calculated as follows.

$$60\% = 100\% - \text{SoC}\ (t)$$

So that

$$\text{SoC}\ (t) = 100\% - 60\% = 40\%$$

Next, using the SoC value of 40% in (2), the primary battery voltage at DoD 60% or SoC 40% can be calculated as follows.

$$40\% = \frac{V_B - 10.8\ V}{13.2\ V - 10.8\ V} \cdot 100\%$$

so that it is obtained

$$V_B = \left\{\frac{40\%}{100\%} \cdot (13.20\ V - 10.8\ V)\right\} + 10.8 = 11.76\ V$$

Using the same calculation method, the relationship between battery voltage (OCV) and the SoC and DoD in this study can be estimated, as shown in Table VIII.

TABLE VIII. THE ESTIMATED BATTERY VOLTAGE AT DOD AND SOC

DoD (%)	SoC (%)	Voltage (V)	
		Primary Battery	*Standby Battery*
0	100	≥13.20	≥13.12
10	90	12.96	12.89
20	80	12.72	12.66
30	70	12.48	12.42
40	60	12.24	12.19
50	50	12.00	11.96
60	40	11.76	11.73
70	30	11.52	11.50
80	20	11.28	11.26

Based on Table VIII, the reference voltage is set to 13.2 V for V_{BHP} on LVD1 and 12.7 V for V_{BHS} on LVD2. The reference voltages for V_{BLP} and V_{BLS} can be calculated based on (4) using the voltage at 60% DoD.

$$V_{BLP} = 2\ (11.76 - 6.02)\ \text{volt} = 11.48\ \text{volt} \approx 11.4\ \text{volt}$$

$$V_{BLS} = 2\ (11.73 - 6.02)\ \text{volt} = 11.42\ \text{volt} \approx 11.4\ \text{volt}$$

Thus, the reference voltage is set to 11.4 V for V_{BLP} on LVD1 and V_{BLS} on LVD2. Rounding to one decimal place in these LVD settings aligns with the output voltage values displayed by the 3-digit 7-segment LEDs on LVD1 and LVD2, as shown in Fig. 8. When the primary battery's initial voltage exceeds 11.4 V, coils EMR1 and EMR2 are energized by the LVD1 output. Consequently, the primary battery disconnects from the SCC but connects to the load via the connectivity of EMR2's CO and NO contacts to discharge. Meanwhile, the standby battery disconnects from the load but connects to the SCC to charge via the connectivity of EMR1's CO and NC contacts. Conversely, when the primary battery's initial voltage is under 11.4 V or drops to 11.4 V, coils EMR1 and EMR2 are de-energized by the LVD1 output. Consequently, the primary battery disconnects from the load but connects to the SCC to charge via the connectivity CO and NC contacts of EMR1. Meanwhile, the standby battery disconnects from the SCC but connects the load to discharge via the connectivity CO and NC contacts of EMR2. Coils EMR1 and EMR2 are resumed energized by the LVD1 output when the primary battery voltage reaches 13.2 V.



Fig. 8. Output voltage displays LVD1 and LVD2

When the standby battery's initial voltage exceeds 11.4 V, coil EMR3 is energized by the LVD2 output. Consequently, the standby battery connects to the load via the CO and NO contacts of the EMR3, discharging when the primary battery charges and charging when the primary battery is discharging. Conversely, when the standby battery's initial voltage is under 11.4 V or drops to 11.4 V, coil EMR3 is de-energized by the LVD2 output. Consequently, the standby battery disconnects from the load via EMR3's NC contact. Coil EMR3 resumes energization by the LVD2 output when the standby battery voltage reaches 12.7 V.

Testing of the battery control system was conducted to evaluate its performance in managing switching between charging and discharging for both the primary and standby batteries, based on battery voltage levels. The results of the battery control system testing are presented in Table IX. Based on the test results in Table IX, the proposed battery control system successfully operated automatic switching between discharging and charging for the primary and standby batteries within a 12 V DC small-scale SAPV system. The two batteries alternated between discharge and charge operations. The primary battery completed its full discharge and charge operation cycles. The standby battery—taking over the load power supply—was successfully prevented from discharging as long as its SoC did not reach the established V_{BH} threshold when the primary battery was charging. This system is simple, economical, and easy to implement, constructed using two LVDs and three EMRs as the main components. The measured battery voltages during the transition from discharging to charging (or vice versa) modes did not always match the established V_{BH} and V_{BL} of the primary or the standby battery.

TABLE IX. THE RESULT OF THE BATTERY CONTROL SYSTEM TESTING

	Battery Voltage (V)		Battery Operation		State
	Primary	*Standby*	*Primary*	*Standby*	
1	12.5	12.4	Discharging	Charging	S1
2	11.5	12.8	Discharging	Charging	S1
3	11.8	12.5	Charging	Discharging	S3
4	13.1	12.3	Charging	Discharging	S3
5	13.1	12.6	Discharging	Charging	S1
6	11.4	13.0	Discharging	Charging	S1
7	11.7	12.8	Charging	Discharging	S3
8	11.8	11.5	Charging	Discharging	S3

EISSN: 2961-872X ●PISSN: 2961-8924●DOI: 10.56741/IISTR.esl.002471

	Battery Voltage (V)		Battery Operation		State
	Primary	*Standby*	*Primary*	*Standby*	
9	11.9	11.8	Charging	Waiting to charge	S4
10	13.1	11.7	Charging	Waiting to charge	S4
11	13.1	11.8	Discharging	Charging	S2
12	11.5	12.0	Discharging	Charging	S2
13	11.7	12.0	Charging	Waiting to charge	S4
14	13.1	11.9	Charging	Waiting to charge	S4
15	13.1	11.9	Discharging	Charging	S2
16	12.8	12.4	Discharging	Charging	S1
17	11.5	12.9	Discharging	Charging	S1
18	11.8	12.6	Charging	Discharging	S3
19	13.1	12.5	Charging	Discharging	S3
20	13.0	12.6	Discharging	Charging	S1
21	11.5	12.8	Discharging	Charging	S1
22	11.9	12.5	Charging	Discharging	S3
23	13.0	11.4	Charging	Waiting to charge	S3
24	13.1	11.5	Discharging	Charging	S2
25	11.5	12.5	Discharging	Charging	S2
26	11.8	12.2	Charging	Discharging	S3
27	12.9	11.3	Charging	Waiting to charge	S4
28	13.2	11.7	Discharging	Charging	S2
29	12.6	12.3	Discharging	Charging	S1
30	11.6	12.8	Charging	Discharging	S3

When the operating mode shifts from discharging to charging, the battery terminal voltage tends to rise. This increase occurs because the battery receives charging current from the SCC; under these conditions, there is no voltage drop caused by discharge current flowing to the load. The charging process raises the battery's electrochemical potential, resulting in a higher measured terminal voltage than during discharging. Conversely, when the battery switches from charging to discharging, the terminal voltage tends to decrease. This happens because during discharge, the battery supplies current to the load, causing a voltage drop across its internal resistance. Furthermore, the energy discharge process triggers electrochemical polarization, which contributes to a lower terminal voltage than the no-load voltage. These phenomena are characteristic of VRLA batteries and demonstrate that terminal voltage is influenced not only by the battery's SoC but also by the direction and magnitude of the current flowing during charging or discharging.

The experimental results demonstrate that the proposed state-based control strategy successfully performs automatic switching between the primary and standby batteries while maintaining uninterrupted power delivery. This performance is consistent with previous studies showing that proper battery management improves the reliability of standalone PV systems [14], [18], [20], [22]. Unlike existing approaches that typically rely on digital controllers, the proposed system achieves this functionality using only LVDs and EMRs. This simpler hardware architecture reduces implementation complexity and cost while maintaining reliable automatic operation for small-scale standalone PV applications.

The proposed charging and discharging strategy is consistent with recommended VRLA battery operating practices by maintaining complete charging-discharging cycles for the primary battery while preventing simultaneous charging and discharging using coordinated relay switching. Such an operating strategy aligns with previous studies showing that shallow cycling, prolonged low State of Charge (SoC), and simultaneous charging and discharging accelerate battery degradation [15], [16], [17]. Nevertheless, further long-term experimental studies are required to evaluate its effectiveness in extending battery service life.

The experimental observation that the measured transition voltages did not always exactly coincide with the predefined threshold values is also consistent with the electrochemical characteristics of VRLA batteries. During charging and discharging, the measured terminal voltage is influenced not only by the battery State of Charge but also by internal resistance, current flow, and electrochemical polarization. Consequently, temporary deviations between the measured terminal voltage and the estimated open-circuit voltage are expected during state transitions [31], [32]. Despite these voltage variations, all observed switching events followed the intended state-transition logic.

IV. Conclusion

This study successfully developed an automatic switching system between primary and standby batteries for a 12 V DC standalone photovoltaic (SAPV) system using a combination of Low-Voltage Disconnect (LVD) devices and Electromechanical Relays (EMRs) with state-based control logic. The proposed system addresses the challenge of battery management in small-scale off-grid PV systems, where existing solutions commonly rely on more complex and costly digital controllers.

Experimental results demonstrate that the proposed system successfully performs four operating states and eight state transitions in accordance with the designed control strategy. The primary battery is prioritized to complete full charge-discharge cycles. In contrast, the standby battery automatically supplies the load during the primary battery charge, thereby maintaining uninterrupted power delivery. In addition, the proposed control strategy effectively prevents simultaneous charging and discharging of the batteries, which may help reduce VRLA battery degradation.

Although the measured transition voltages did not always exactly match the predefined threshold values because of the dynamic characteristics of VRLA batteries during charging and discharging, the control system operated consistently with the intended state-transition logic. Therefore, the proposed LVD-EMR-based control system provides a simple, low-cost, and practical alternative for battery management in small-scale SAPV systems, with the potential to improve battery reliability and service life.

Acknowledgment

The authors acknowledge the Faculty of Engineering, University of Bengkulu, for funding this research through the DIPA (Budget Implementation List) program under Contract Number 7060/UN30.13/PG/2025.

References

[1] C. F. Nugraha, L. Subekti, A. A. Muthahhari, B. E. Prasetyo, and R. F. S. Budi, 'A Sustainable Hybrid Off-Grid System Design for Isolated Island Considering Techno-Economic and Frequency Stability Analysis', *JAETS*, vol. 6, no. 1, pp. 444–464, 2024, doi: https://doi.org/10.37385/jaets.v6i1.4892.

[2] H. Wirawan and Y. M. L. Gultom, 'The effects of renewable Energy-based Village Grid Electrification on Poverty Reduction in Remote Areas: The Case of Indonesia', *Energy for Sustainable Development*, vol. 62, pp. 186–194, 2021, doi: 10.1016/j.esd.2021.04.006.

[3] S. Ariyani, D. A. Wicaksono, Fitriana, R. Taufik, and Germenio, 'Studi Perencanaan dan Monitoring System Pembangkit Listrik Tenaga Surya di Remote Area', *Techné*, vol. 20, no. 2, pp. 113–124, 2021, doi: https://doi.org/10.31358/techne.v20i2.273.

[4] G. Sihombing and Suwarno, 'Pemanfaatan Energi Terbarukan Of Grid di Daerah Terpencil Indonesia', *E –Link*, vol. 16, no. 2, pp. 40–53, 2021, doi: https://doi.org/10.30587/e-link.v16i2.3027.

[5] H. Lestari, M. Arentsen, H. Bressers, B. Gunawan, J. Iskandar, and Parikesit, 'Sustainability of Renewable Off-Grid Technology for Rural Electrification : A Comparative Study Using the IAD Framework', *Sustainability*, vol. 10, no. 12, p. 4512, 2018, doi: https://doi.org/10.3390/su10124512.

[6] H. El-houari *et al.*, 'Design, Simulation, and Economic Optimization of an Off -Grid Photovoltaic System for Rural Electrification', *Energies*, vol. 12, no. 24, p. 4735, 2019, doi: https://doi.org/10.3390/en12244735.

[7] D. F. Silalahi, A. Blakers, M. Stocks, B. Lu, C. Cheng, and L. Hayes, 'Indonesia's Vast Solar Energy Potential', *Energies*, vol. 14, no. 17, 2021, doi: 10.3390/en14175424.

[8] T. Sutikno, A. C. Subrata, and M. H. Jopri, 'Milestone of the Most Used Maximum Power Point Tracking in Solar Harvesting System', *IJPEDS*, vol. 13, no. 3, pp. 1277–1284, 2022, doi: 1http://doi.org/10.11591/ijpeds.v13.i3.pp1277-1284.

[9] I. P. G. I. Dwipayana, I. N. S. Kumara, and I. N. Setiawan, 'Status of Battery in Indonesia to Support Application of Solar PV with Energy Storage', *Journal of Electrical, Electronics and Informatics*, vol. 5, no. 1, pp. 29–40, 2021, doi: https://doi.org/10.24843/jeei.2021.v05.i01.p06.

[10] Y. Yu *et al.*, 'Constructing Accurate Equivalent Electrical Circuit Models of Lithium Iron Phosphate and Lead – Acid Battery Cells for Solar Home System Applications', *Energies*, vol. 11, no. 9, p. 2305, 2018, doi: https://doi.org/10.3390/en11092305.

[11] K. Bedoud, H. Merabet, and T. Bahi, 'Power Control Strategy of a Photovoltaic System with Battery Storage System', *Journal of Engineering and Applied Science*, vol. 69, no. 116, pp. 1–20, 2022, doi: https://doi.org/10.1186/s44147-022-00163-8.

[12] R. G. Charles, M. L. Davies, P. Douglas, I. L. Hallin, and I. Mabbett, 'Sustainable Energy Storage for Solar Home Systems in Rural Sub-Saharan Africa - A Comparative Examination of Lifecycle Aspects of Battery Technologies for Circular Economy, With Emphasis on The South African Context', *Energy*, vol. 166, pp. 1207–1215, 2019, doi: https://doi.org/10.1016/j.energy.2018.10.053.

[13] F. Antonanzas-Torres, J. Antonanzas, and J. Blanco-Fernandez, 'Environmental Impact of Solar Home Systems in Sub-Saharan Africa', *Sustainability*, vol. 13, no. 17, p. 9708, 2021, doi: https://doi.org/10.3390/su13179708.

[14] S. Jain, S. Dhara, and V. Agarwal, 'A Voltage-Zone Based Power Management Scheme With Seamless Power Transfer Between PV-Battery for OFF-Grid Stand-Alone System', *IEEE Transactions on Industry Applications*, vol. 57, no. 1, pp. 754–763, 2021, doi: https://doi.org/10.1109/TIA.2020.3031265.

[15] M. Wieczorek, S. Wodyk, R. Poliszkiewicz, and P. Witaszek, 'The Influence of Current in Off-Grid PV Systems on Lead – Acid Battery Lifetime and Hybridization with LFP Lattery as Solution', *Energy Reports*, vol. 9, no. 10, pp. 766–773, 2023, doi: https://doi.org/10.1016/j.egyr.2023.05.213.

[16] N. Shamim, V. V. Viswanathan, V. L. Sprenkle, E. C. Thomsen, G. Li, and D. M. Reed, 'Valve Regulated Lead Acid Battery Evaluation under Peak Shaving and Frequency Regulation Duty Cycles', *Energies*, vol. 15, no. 9, 2022, doi: 10.3390/en15093389.

[17] P. T. Thong *et al.*, 'Cycle Performance Analysis of Lead–carbon Electrode Under High-load Conditions for Automotive Battery Applications', *Journal of Power Sources*, vol. 580, p. 233291, 2023, doi: 10.1016/j.jpowsour.2023.233291.

[18] S. Chauhan and BhimSingh, 'Control of Solar PV-Integrated Battery Energy Storage System for Rural Area', *IET Renewable Power Generation*, vol. 15, pp. 1030–1045, 2021, doi: https://doi.org/10.1049/rpg2.12086.

[19] G. V. N. Harshitha and K. N. Sujatha, 'Standalone PV Fed Electric Vehicle Battery Charging System', *International Transactions on Electrical Engineering and Computer Science*, vol. 4, no. 1, pp. 13–24, 2025, doi: https://doi.org/10.62760/iteecs.4.1.2025.128.

[20] P. K. Sahu, S. Jena, and B. C. Babu, 'Power Management and Bus Voltage Control of a Battery Backup-Based Stand-Alone PV System.', *Electrical Engineering*, vol. 104, pp. 97–110, 2022, doi: https://doi.org/10.1007/s00202-021-01391-6.

[21] J. L. Seguel and S. I. J. Seleme, 'Robust Digital Control Strategy Based on Fuzzy Logic for a Solar Charger of VRLA Batteries', *Energies*, vol. 14, no. 4, p. 1001, 2021, doi: https://doi.org/10.3390/en14041001.

[22] S. Chtita, A. Derouich, A. El Ghzizal, and S. Motahhir, 'An Improved Control Strategy for Charging Solar Batteries in Off-Grid Photovoltaic Systems', *Solar Energy*, vol. 220, pp. 927–941, 2021, doi: https://doi.org/10.1016/j.solener.2021.04.003.

[23] K. Chao and B. Huang, 'Quantitative Design for the Battery Equalizing Charge/Discharge Controller of the Photovoltaic Energy', *Batteries*, vol. 8, no. 12, p. 278, 2022, doi: https://doi.org/10.3390/batteries8120278.

[24] W. He, M. J. A. Baig, and M. T. Iqbal, 'An Internet of Things — Supervisory Control and Data Acquisition (IoT-SCADA) Architecture for Photovoltaic System Monitoring , Control , and Inspection in Real Time', *Electronics*, vol. 14, no. 1, p. 42, 2025, doi: https://doi.org/10.3390/electronics14010042.

[25] R. S. Rinaldi, A. Herawati, I. N. Anggraini, and Mawardi, 'Design of an Automatic Relay-Based Switching System Using Battery and PV Voltage in Off-Grid Solar PV Lighting', *ECOTIPE*, vol. 13, no. 1, pp. 111–120, 2026, doi: https://doi.org/10.33019/jurnalecotipe.v13i1.4594.

[26] M. J. Milovanović, J. N. Radosavljević, and B. D. Perović, 'Experimental Comparative Analysis of Electromechanical , Static and Microprocessor Relay Protection Technologies', *ICCK Transactions on Electric Power Networks and Systems*, vol. 2, no. 2, pp. 79–88, 2026, doi: http://dx.doi.org/10.62762/TEPNS.2026.788018.

[27] A. Kern, J. X. Johnson, and J. L. Mathieu, 'Environmental Impacts of Using Energy Storage Aggregations to Provide Multiple Services', *Proceedings of the 52nd Hawaii International Conference on System Sciences*, vol. 2019-Janua, pp. 3580–3589, 2019, doi: 10.24251/hicss.2019.433.

[28] M. Shabani, M. Shabani, F. Wallin, E. Dahlquist, and J. Yan, 'Smart and Optimization-based Operation Scheduling Strategies for Maximizing Battery Profitability and Longevity in Grid-connected Application', *Energy Conversion and Management: X*, vol. 21, no. December 2023, p. 100519, 2024, doi: 10.1016/j.ecmx.2023.100519.

[29] J. Vaicys, S. Gudzius, A. Jonaitis, R. Rackiene, A. Blinov, and D. Peftitsis, 'A Case Study of Optimising Energy Storage Dispatch: Convex Optimisation Approach with Degradation Considerations', *Journal of Energy Storage*, vol. 97, p. 112941, 2024, doi: 10.1016/j.est.2024.112941.

[30] H. R. Iskandar *et al.*, 'Analisis Performa Baterai Jenis Valve Regulated Lead Acid Pada PLTS Off-Grid 1 Kwp', *Jurnal Teknologi*, vol. 13, no. 2, pp. 129–140, 2021, doi: 10.24853/jurtek.13.2.129-140.

[31] M. I. Wahyuddin, U. Darusalam, P. S. Priambodo, and H. Sudibyo, 'Battery State of Charge Estimation Based on Internal Resistance and Recovery Effect Analysis', *International Energy Journal*, vol. 22, no. 4, pp. 357–366, 2022, doi: https://doi.org/10.64289/iej.22.0412.2796374.

[32] A. Qurthobi, A. B. K. Pambudi, D. Darmawan, and R. F. Iskandar, 'Correlation between Battery Voltage under Loaded Condition and Estimated State of Charge at Valve-Regulated Lead Acid Battery on Discharge Condition using Open Circuit Voltage Method', *International Journal of Power Electronics and Drive Systems (IJPEDS)*, vol. 9, no. 1, pp. 357–364, 2018, doi: https://doi.org/10.11591/ijpeds.v9n1.pp357-364.

[33] H. Zhang, Q. Wang, and Y. You, 'Tolerance of Electromagnetic Relay to Voltage Sags and Short Interruptions', *Frontiers in Energy Research*, vol. 9, no. 766472, pp. 1–12, 2021, doi: https://doi.org/10.3389/fenrg.2021.766472.

[34] Anonim, 'Shoto/6-FMX-100B', Direct INDUSTRY. Accessed: Mar. 02, 2025. [Online]. Available: https://pdf.directindustry.com/pdf/shoto-shuangdeng-group-company-limited/6-fmx-100b/163966-954795.html.

 EISSN: 2961-872X ●PISSN: 2961-8924●DOI: 10.56741/IISTR.esl.002471